



Can Empirical Algorithms Successfully Estimate Aragonite Saturation State in the Subpolar North Atlantic?

Daniela Turk^{1,2*}, Michael Dowd³, Siv K. Lauvset^{4,5}, Jannes Koelling⁶, Fernando Alonso-Pérez⁷ and Fiz F. Pérez⁷

¹ Department of Oceanography, Dalhousie University, Halifax, NS, Canada, ² Lamont-Doherty Earth Observatory, Columbia University, Palisades, NY, United States, ³ Department of Mathematics and Statistics, Dalhousie University, Halifax, NS, Canada, ⁴ Uni Research Klima, Bjerknes Centre for Climate Research, Bergen, Norway, ⁵ Geophysical Institute, University of Bergen and Bjerknes Centre for Climate Research, Bergen, Norway, ⁶ Scripps Institution of Oceanography, La Jolla, CA, United States, ⁷ Departamento de Oceanografía, Instituto de Investigaciones Marinas (CSIC), Vigo, Spain

OPEN ACCESS

Edited by:

Gilles Reverdin,
Centre National de la Recherche
Scientifique (CNRS), France

Reviewed by:

Fabien Roquet,
Stockholm University, Sweden
Ute Schuster,
University of Exeter, United Kingdom

*Correspondence:

Daniela Turk
daniela.turk@dal.ca

Specialty section:

This article was submitted to
Ocean Observation,
a section of the journal
Frontiers in Marine Science

Received: 21 August 2017

Accepted: 15 November 2017

Published: 01 December 2017

Citation:

Turk D, Dowd M, Lauvset SK,
Koelling J, Alonso-Pérez F and
Pérez FF (2017) Can Empirical
Algorithms Successfully Estimate
Aragonite Saturation State in the
Subpolar North Atlantic?
Front. Mar. Sci. 4:385.
doi: 10.3389/fmars.2017.00385

The aragonite saturation state (Ω_{Ar}) in the subpolar North Atlantic was derived using new regional empirical algorithms. These multiple regression algorithms were developed using the bin-averaged GLODAPv2 data of commonly observed oceanographic variables [temperature (T), salinity (S), pressure (P), oxygen (O_2), nitrate (NO_3^-), phosphate (PO_4^{3-}), silicate ($Si(OH)_4$), and pH]. Five of these variables are also frequently observed using autonomous platforms, which means they are widely available. The algorithms were validated against independent shipboard data from the OVIDE2012 cruise. It was also applied to time series observations of T, S, P, and O_2 from the K1 mooring ($56.5^\circ N$, $52.6^\circ W$) to reconstruct for the first time the seasonal variability of Ω_{Ar} . Our study suggests: (i) linear regression algorithms based on bin-averaged carbonate system data can successfully estimate Ω_{Ar} in our study domain over the 0–3,500 m depth range ($R^2 = 0.985$, RMSE = 0.044); (ii) that Ω_{Ar} also can be adequately estimated from solely non-carbonate observations ($R^2 = 0.969$, RMSE = 0.063) and autonomous sensor variables ($R^2 = 0.978$, RMSE = 0.053). Validation with independent OVIDE2012 data further suggests that; (iii) both algorithms, non-carbonate (MEF = 0.929) and autonomous sensors (MEF = 0.995) have excellent predictive skill over the 0–3,500 m depth range; (iv) that in deep waters (>500 m) observations of T, S, and O_2 may be sufficient predictors of Ω_{Ar} (MEF = 0.913); and (v) the importance of adding pH sensors on autonomous platforms in the euphotic and remineralization zone (<500 m). Reconstructed Ω_{Ar} at Irminger Sea site, and the K1 mooring in Labrador Sea show high seasonal variability at the surface due to biological drawdown of inorganic carbon during the summer, and fairly uniform Ω_{Ar} values in the water column during winter convection. Application to time series sites shows the potential for regionally tuned algorithms, but they need to be further compared against Ω_{Ar} calculated by conventional means to fully assess their validity and performance.

Keywords: aragonite saturation state, empirical algorithms, autonomous sensors, commonly observed oceanic variables, GLODAPv2, subpolar North Atlantic

INTRODUCTION

Complex horizontal and vertical circulation in the subpolar North Atlantic has the potential to influence global ocean circulation and climate patterns. Deep water formation coupled with strong winds, and high rates of primary production in spring and summer result in this region of the subpolar North Atlantic acting as a strong sink for atmospheric carbon dioxide (DeGrandpre et al., 2006; Pérez et al., 2008). Over the past two decades an increase in surface water $p\text{CO}_2$ at a rate greater than that of the atmosphere has been observed in the Irminger Sea (Olafsson et al., 2009; Bates et al., 2014). In response to this increasing $p\text{CO}_2$, the surface water pH and the aragonite saturation states (Ω_{Ar}) show a decreasing trend (Vazquez-Rodriguez et al., 2012; García-Ibáñez et al., 2016). Pérez (2016), using the RCP8.5 scenario of the IPCC (2013), predicted that aragonite undersaturation ($\Omega_{Ar} < 1$) in the Irminger basin would likely occur between 2050 and 2065, at atmospheric CO_2 levels between 510 and 640 ppm.

Most of the historical measurements of inorganic carbon (García-Ibáñez et al., 2016; Olsen et al., 2016) in the Irminger and Labrador basins have occurred on a few repeated transects over time, or at specific locations (Olafsson et al., 2009; Azetsu-Scott et al., 2010). The subpolar North Atlantic remains undersampled with respect to its scales of variability (Fröb et al., accepted), but novel sensor packages now being deployed on autonomous platforms (e.g., profiling floats, gliders, moorings) have the potential to dramatically increase observational coverage in time and space. Unfortunately, most of these platforms do not directly provide the set of two inorganic carbon measurements commonly used to derive Ω_{Ar} . This argues for a need to develop regional predictive algorithms to determine estimates of key water chemistry variables, such as Ω_{Ar} , from information contained in the measurements of commonly observed oceanic non-carbonate variables such as temperature (T), salinity (S), pressure (P), oxygen (O_2), and nutrients and/or variables that can be measured by autonomous sensors.

Previous studies have used multiple linear regression models (MLR) to estimate inorganic carbon variables from hydrographic measurements (Juraneck et al., 2009, 2011; Kim et al., 2010; Alin et al., 2012; Bostock et al., 2013; Williams et al., 2016; Carter et al., 2017). These were applied to different data sets (hydrographic surveys, time-series, profiling floats, climatology) in order to reconstruct estimates of the natural variability of carbon variables. Juraneck et al. (2009, 2011) used hydrographic surveys of T and O_2 to estimate Ω_{Ar} off the Oregon coast, and Argo profiling float T and O_2 profiles to estimate pH and Ω_{Ar} in the northeastern subarctic Pacific Ocean. Alin et al. (2012) reconstructed pH, carbonate saturation states, carbonate ion concentration, total dissolved inorganic carbon (TCO_2), and total alkalinity (TALK) in the California Current System from T, O_2 , S, and density. Williams et al. (2016) estimated pH in the Pacific sector of Southern Ocean from T, S, O_2 , P, and nitrate (NO_3^-). Furthermore, Bostock et al. (2013) used T, S, and O_2 to estimate TALK and TCO_2 in the intermediate and deep waters of the Southern Hemisphere, while Kim et al. (2010) used T, P, and O_2 to estimate Ω_{Ar} in the Sea of Japan.

All these studies demonstrated that Ω_{Ar} can be robustly determined from measurements of commonly observed and/or non-carbonate oceanic variables and that MLR models provide a valuable tool for reconstructing Ω_{Ar} where direct observations of carbonate variables are not available. It is, however, expected that relationships between Ω_{Ar} and other variables will vary among different parts of the ocean suggesting a need for development of regional models. To our knowledge, such regional models have not been developed in the subpolar North Atlantic. While clearly not replacing direct measurements of inorganic carbon variables, these approaches produce estimates of Ω_{Ar} , including calculations of error, which can greatly expand the information in both space (e.g., in undersampled areas), and in time (e.g., during the wintertime where almost no inorganic carbon measurements are available). This will allow for better detection and attribution of ocean acidification (OA) related processes to anthropogenic CO_2 and identification of potential OA “hot spots,” while also improving the understanding of complex patterns and relationships between physical and chemical changes (e.g., during deep water convection, extreme wind events or fresh water input, and eddy activity) and the marine communities affected by OA. Regionally tuned empirical algorithms can also provide guidance for optimal placement (horizontal and depth) of additional autonomous platforms in the subpolar North Atlantic that augment current and planned ship surveys [e.g., Observatoire de la variabilité interannuelle et décennale en Atlantique Nord (OVIDE), AR7W, RedFish] and existing time-series [e.g., K1 mooring, Central Irminger Sea mooring (CIS), Overturning in the Subpolar North Atlantic Program (OSNAP)].

Quantifying predictive skill is key to assessing the effectiveness of any empirical algorithm. This includes the goodness of fit for the regressions of Ω_{Ar} on oceanographic variables and skill assessment metrics (Stow et al., 2009). These can help guide improvements in model structure, as well as aid in recognizing model limitations. Another important aspect of predictive skill is an empirical algorithm’s ability to successfully predict “out of sample” (i.e., validation of the algorithm on an independent data not used in building the original regression model). This is particularly important when models are used as tools to support decision-making. While common in the statistical literature, such independent validation has not been adequately addressed by most of the previous studies in oceanography.

The goal of this study is to investigate the predictive skill of commonly observed non-carbonate and autonomous sensor oceanographic variables [T, S, P, O_2 , NO_3^- , phosphate (PO_4^{3-}), and silicate ($\text{Si}(\text{OH})_4$), pH] in determining a key water chemistry variable (Ω_{Ar}) in the subpolar North Atlantic. This region is of high oceanographic interest due to its role in Atlantic Meridional Overturning (Jackson et al., 2016) and a major carbon dioxide sink (Sabine et al., 2004). The rationale for this work is to assess the potential for autonomous sensors and biogeochemical models to monitor Ω_{Ar} in undersampled regions of the ocean and to provide information to the research community for cost and benefit analysis to support decisions on selection of optimal sets of shipboard measurements and set of sensors for outfitting autonomous platforms. Regional algorithms are necessary as the empirical relationships between Ω_{Ar} and oceanographic

variables would be expected to vary over broad domains with a wide range of oceanographic conditions (e.g., such as the whole North Atlantic). The specific objectives are to (1) develop regional empirical algorithms for the subpolar North Atlantic to determine Ω_{Ar} using existing data from GLODAPv2, which has not been done before; and (2) validate the algorithms against independent shipboard data (from the OVIDE2012 cruise) to assess its performance and to improve best practices in skill assessment methodology. As an illustration of how the algorithms trained with GLODAPv2 data can be applied to a set of commonly measured non-carbon variables we use the derived empirical algorithm with a time series data from Irminger Sea site, and from a mooring (Station K1 in the Labrador Sea), and estimate for the first time the variability of Ω_{Ar} over a full seasonal cycle.

DATA

GLODAPv2 Data

Observations of oceanographic non-carbonate variables [T ($^{\circ}$ C), S, P (dbar), O_2 ($\mu\text{mol kg}^{-1}$), NO_3^- ($\mu\text{mol kg}^{-1}$), PO_4^{3-} ($\mu\text{mol kg}^{-1}$), Si(OH)_4 ($\mu\text{mol kg}^{-1}$)] and inorganic carbonate variables [TALK ($\mu\text{mol kg}^{-1}$), pH (at *in situ* T and P), and Ω_{Ar}] were extracted from Global Ocean Data Analysis Project version 2 (GLODAPv2; Olsen et al., 2016). The input for our analysis are the vertically interpolated, horizontally bin averaged bottle data extracted from the mapped GLODAPv2 product (Lauvset et al., 2016). Each of these bin-averaged data points comes with an associated standard deviation, as well as the number of data in the bin. For further details on this data product the reader is referred to Lauvset et al. (2016) and the published metadata (available here: <https://www.nodc.noaa.gov/archive/arc0107/0162565/1.1/data/0-data/mapped/>). Note that in order to eliminate biases due to variable spatial and temporal resolution of the bottle data and an anthropogenically-driven trend, both the pH and Ω_{Ar} data were normalized to year 2002 before binning and averaging. The GLODAPv2 normalization was done by using anthropogenic carbon calculated with the transit time distribution (TTD) method (Hall et al., 2002; Waugh et al., 2006) to correct TCO_2 to year 2002. Ω_{Ar} was then calculated from the normalized TCO_2 . The method is thoroughly described in Lauvset et al. (2016). The bin-averaged data were also used as the basis for the 1° latitude and longitude spatial statistical mapping by Lauvset et al. (2016), but we note that this global mapped product had large spatial scales incompatible with our limited regional focus.

Ω_{Ar} (at *in situ* T and P) in GLODAPv2 was calculated from the TCO_2 (normalized to year 2002 to remove anthropogenic influence) and TALK. pH was calculated from the TCO_2 (normalized to year 2002 to remove anthropogenic influence) and TALK at both *in situ* T and P, and at constant T (25°C) and P (0 dbar). All calculations for the carbonate system in GLODAPv2 were performed using the MATLAB version (van Heuven et al., 2009) of CO_2SYS (Lewis and Wallace, 1998) using T, S, P, PO_4^{3-} , and Si(OH)_4 , the dissociation constants of Lueker et al. (2000) for carbonate, Dickson (1990) for sulfate, and the total borate-salinity relationship of Uppström (1974). The uncertainty in

calculated Ω_{Ar} was about 0.05. For further details, see Olsen et al. (2016).

The geographical domain of our study was adapted from the southwestern portion of the Longhurst ARCT biogeochemical province (Longhurst, 1995; **Figure 1**-black line), and designed to reflect the approximate boundaries of the Irminger and most of the Labrador Sea. For each variable approximately 1630 data points in this domain were extracted from GLODAPv2 and used to develop empirical algorithms using a multiple linear regression (MLR) model (see section Methods). Note that the GLODAPv2 data (**Figure 1**-blue dots) has a well-recognized seasonal bias as this region of the subpolar North Atlantic is almost exclusively sampled in May–August (boreal summer). The bin-averaged data used here are thus representative of the summer season.

Shipboard Measurements

To validate the empirical algorithms derived from the regression analysis of the GLODAPv2 data [see section Multiple Linear Regression (MLR) Algorithms (Training)], we used Conductivity-Temperature-Depth (CTD) profiles and water samples for nutrients [NO_3^- ($\mu\text{mol kg}^{-1}$), PO_4^{3-} ($\mu\text{mol kg}^{-1}$), and Si(OH)_4 ($\mu\text{mol kg}^{-1}$)], and inorganic carbon (TALK and pH) from the OVIDE section across the Irminger Sea in summer 2012 (**Figure 1**-pink circles). These data were not included in GLODAPv2, because they were not submitted in time for inclusion in the database, and hence represent an independent data set. For the OVIDE2012 cruise, water samples were drawn at 108 stations from 0 to 5,400 m depth. TALK was analyzed by single point titration (Mintrop et al., 2000; Pérez and Fraga, 2007) and calibrated with certified reference materials (CRMs) (Dickson et al., 2007) with overall accuracy of $4 \mu\text{mol kg}^{-1}$. pH was determined at T = 25°C and P = 1 atm with a spectrophotometric method with uncertainty of 0.0055 pH units

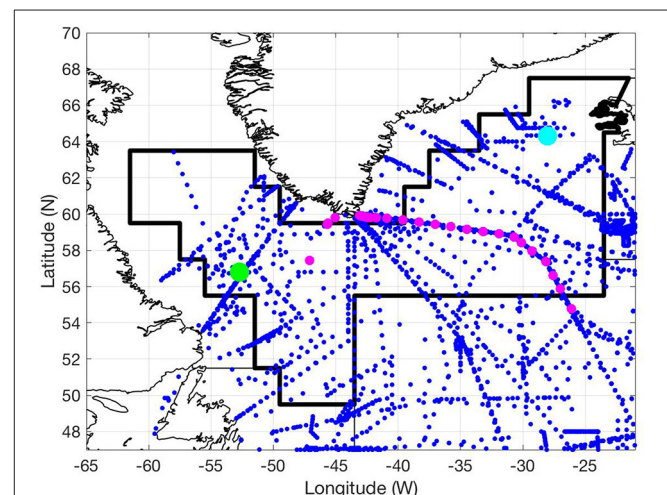


FIGURE 1 | Map of the northern North Atlantic, showing GLODAPv2 bottle data locations (blue dots) with OVIDE2012 cruise stations (pink dots) and K1 mooring location (green dot) and Irminger Sea site (light blue dot). Black line represents the southwestern portion of Longhurst Atlantic-Arctic (ARCT) province, which is the study domain.

(Clayton and Byrne, 1993). Further details on the analysis of inorganic carbon is described in García-Ibáñez et al. (2016). As TCO_2 was not measured at OVIDE2012, Ω_{Ar} was calculated from TALK and pH (total scale, at *in situ* T and P), and T, S, P, PO_4^{3-} , and Si(OH)_4 using the same MATLAB version of CO_2SYS (van Heuven et al., 2009) and constants (Uppström, 1974; Dickson, 1990; Lueker et al., 2000) as used in GLODAPv2. The estimated uncertainty in calculated Ω_{Ar} using a perturbation (Monte Carlo) method and uncertainties of $6 \mu\text{mol kg}^{-1}$ for TALK and 0.01 for pH, were between 0.020 and 0.056 (Perez, personal communication). Nutrient analyses were performed using a SKALAR segmented flow auto-analyser, and oxygen samples were analyzed by the Winkler method. Details of the analysis are given in the CATARINA Cruise report (<https://cchdo.ucsd.edu/cruise/29AH20120622>). Given that there is a non-negligible uncertainty associated with the calculation of Ω_{Ar} , and that the calculation from TALK and pH yield slightly different answers compared to using the TALK and TCO_2 combination as in GLODAPv2, this adds further rationale for performing skill assessment using independent validation (i.e., while every effort is made to ensure consistency, independently collected data will always have its own unique features). We also note the observed decrease in pH [$-0.025 \text{ pH decade}^{-1}$ in the Irminger Sea, Bates et al. (2014)] as a consequence of increase in TCO_2 since 2002 due to invasion of anthropogenic CO_2 . For validation of the regression analysis we extracted the subset of OVIDE2012 data from 0 to 3,500 m at those stations and depths where the complete set of analysis variables was available (303 points for each variable).

Time Series

As an illustration of how the algorithms trained with GLODAPv2 data can be applied to a set of commonly measured non-carbon variables to predict seasonal variability of Ω_{Ar} in the surface waters, we used time series data of T, S, P, and O_2 at 10 and 100 m depth from two sites in subpolar North Atlantic (Figure 1): (1) Irminger Sea site (64.3°N , 28°W , Olafsson, 2016), and (2) the K1 mooring (56.5°N , 52.6°W) in Labrador Sea.

For Irminger Sea site, we used T, S, P, and O_2 data from 2010 to 2012, measured four times per year (February, May, August, November). We also used T, S, P, TCO_2 , pCO_2 , PO_4^{3-} , and Si(OH)_4 to compute Ω_{Ar} using CO_2SYS for comparison with estimated Ω_{Ar} . For the K1 mooring we have high frequency T, S, P, and O_2 data from August 2014 to March 2015. O_2 measurements from the K1 mooring were inter-calibrated when the mixed layer encompassed both sensors, and matched to a CTD profile taken prior to deployment. The details on measurements are described in Koelling et al. (2017). Observations of inorganic carbon variables at K1 mooring location during our time-series observations were not available.

METHODS

The saturation state (Ω_{Ar}) for the aragonite is calculated as:

$$\Omega_{Ar} = [\text{Ca}^{2+}][\text{CO}_3^{2-}]/K'_{sp} \quad (1)$$

where $[\text{Ca}^{2+}]$ is concentration of calcium ions, $[\text{CO}_3^{2-}]$ is concentration of carbonate ions and K'_{sp} is the stoichiometric solubility product for aragonite. $[\text{Ca}^{2+}]$ changes in seawater are related to S, but they are small, therefore Ω_{Ar} is largely determined by changes in $[\text{CO}_3^{2-}]$ and K'_{sp} . $[\text{CO}_3^{2-}]$ can be calculated from TCO_2 and TALK, where TCO_2 varies (non-linear) with physical conditions and biological activity (Barbero et al., 2011) and TALK with T and S (linear) (Lee et al., 2006). K'_{sp} is a function (non-linear) of T, S, and P. In the open ocean, we expect (1) TCO_2 to increase with higher uptake of nutrients and decrease with production of O_2 , (2) TALK to increase with T and S, and (3) K'_{sp} to decrease with T and increase with P and S. We thus anticipate that Ω_{Ar} will also vary with all these variables (most likely non-linear); generally to increase with T, O_2 , and pH, and decrease with P and nutrients. The relationship with S is harder to predict, as well as whether the relationships of these variables with non-conservative quantity, such as Ω_{Ar} could be predicted with linear function.

Multiple Linear Regression (MLR) Algorithms (Training)

MLR was used to develop a predictive relationship for Ω_{Ar} in the subpolar North Atlantic in 0–3,500 m, which is referred to as the “training” of the algorithm. MLR used GLODAPv2 Ω_{Ar} as the response variable and a subset of the GLODAPv2 data [T, S, P, pH, TALK, O_2 , NO_3^- , PO_4^{3-} , and Si(OH)_4] as predictor variables, all of which are potentially readily measureable quantities. The regression equation for the full model, which includes both non-carbonate variables and the autonomous sensor variables is:

$$\Omega_{Ar} = \beta_0 + \beta_1 T + \beta_2 S + \beta_3 P + \beta_4 \text{pH} + \beta_5 \text{O}_2 + \beta_6 \text{NO}_3^- + \beta_7 \text{PO}_4^{3-} + \beta_8 \text{Si(OH)}_4 + e \quad (2)$$

where β_i are the regression coefficients (with β_0 representing the intercept) and e is the error term. Note that we do not include TALK in the full model of Equation (2), but instead also consider a separate model with those predictor variables that are used as inputs to CO_2SYS to calculate Ω_{Ar} [i.e., T, S, P, TALK, pH, PO_4^{3-} , and Si(OH)_4]:

$$\Omega_{Ar} = \beta_0 + \beta_1 T + \beta_2 S + \beta_3 P + \beta_4 \text{pH} + \beta_5 \text{TALK} + \beta_6 \text{PO}_4^{3-} + \beta_7 \text{Si(OH)}_4 + e \quad (3)$$

To account for both the sampling density and data spread, all regressions were weighted by the inverse of standard error making the weighting proportional to the square root of the number of data points per bin. Note that in all cases considered here, regression output yield error estimates for the regression parameters, as well as confidence and prediction intervals for estimated Ω_{Ar} .

For reasons of parsimony and interpretability we have chosen only to consider the oceanographic predictor variables in their original forma and not to consider higher order regression models wherein the predictor variables are combined into products and nonlinear polynomial relations are used. Similarly, we have explicitly decided not to include latitude and longitude as predictor variables. The rationale is that the regional domain

for analysis has been chosen so that relationships should be relatively homogenous within it, and also that spatial variations (as embodied in latitude and longitude as predictors) can be easily confounded with changes in the primary oceanographic variable.

Two regression model building strategies were undertaken to identify the best set of oceanographic variables useful in predicting Ω_{Ar} . These strategies broadly correspond to (i) unsupervised and (ii) supervised learning (e.g., see Hastie et al., 2009). We used two types of unsupervised model building approaches. The first of these is “all possible regressions.” This approach considers all possible subsets of the predictor variables and can identify the regression model that has the best fit for a given number of predictor variables (i.e., the best regression based on one predictor, two predictors, etc.), as well as allow for assessment of the tradeoff in including different subsets of the available predictor variables. The second unsupervised approach was an automated selection of a set of best predictor variables for Ω_{Ar} based on the statistical model building technique of stepwise regression (Montgomery et al., 2015). Here, we performed stepwise predictor variable selection based on information criteria wherein regression fit (as measured by the coefficient of determination, R^2) is balanced against model complexity (the number of predictor variables). We used the Bayesian Information Criterion (BIC) (Box et al., 1994), since this provides for a relatively strong complexity penalty relative to other information criteria (Plancherel et al., 2013). Three established stepwise approaches were implemented: forward selection, backward elimination, and forward/backward combination. For details on these techniques, the interested reader is referred to Montgomery et al. (2015), or most textbooks on multiple regression.

This unsupervised approach, however, does not take into account which variables are easy to measure, or which might be readily available through existing instruments or monitoring programs. Hence, we also use a scenario based, or “supervised learning,” approach to predict Ω_{Ar} . Three cases are considered: Scenario 1 uses non-carbonate variables [T, S, P, NO_3^- , PO_4^{3-} , Si(OH)_4] only; Scenario 2 uses variables that can be measured by autonomous sensors (T, S, P, O_2 , pH, NO_3^-); and Scenario 3, designed to see how well a regionally tuned MLR model can represent the carbonate system in terms of predicting Ω_{Ar} using the inputs to CO_2SYS [i.e., T, S, P, TALK, pH, PO_4^{3-} , and Si(OH)_4], and here is named the “ CO_2SYS model.” For the first two scenarios we examine subsets of predictors to identify key variables. This strategy provides useful information toward a cost-benefit analysis to inform decisions on prioritization of shipboard measurements and outfitting of autonomous platforms.

Validation

The empirical algorithms were evaluated in terms of their ability to predict “out of sample,” i.e., validation based on an independent data set that was not used in training the regression model. Here an independent data set from the OVIDE2012 cruise (Figure 1) was used for validation. Specifically, the derived algorithms were applied to (subsets) of the predictor variables (Table 3) measured on the OVIDE2012 cruise. Predicted Ω_{Ar}

from algorithms trained with GLODAPv2 climatological data were compared to “observed” Ω_{Ar} as calculated from carbon parameters (pH and TALK) measured on the OVIDE2012 cruise. The quantitative metrics used to assess validation performance followed Stow et al. (2009), and a detailed interpretation is given there. Metrics included: correlation (r), root mean squared error (RMSE), the reliability index (RI), the average error (AE), the average absolute error (AAE), and the modeling efficiency (MEF). We have adopted the following quantification for MEF thresholds: MEF < 0.2 (poor), MEF 0.2–0.5 (good), MEF 0.5–0.65 (very good), and MEF > 0.65 (excellent; Allen et al., 2007; Nondal et al., 2009). These metrics, taken together, act to assess the bias and variability associated with applying the empirical algorithms to independent data.

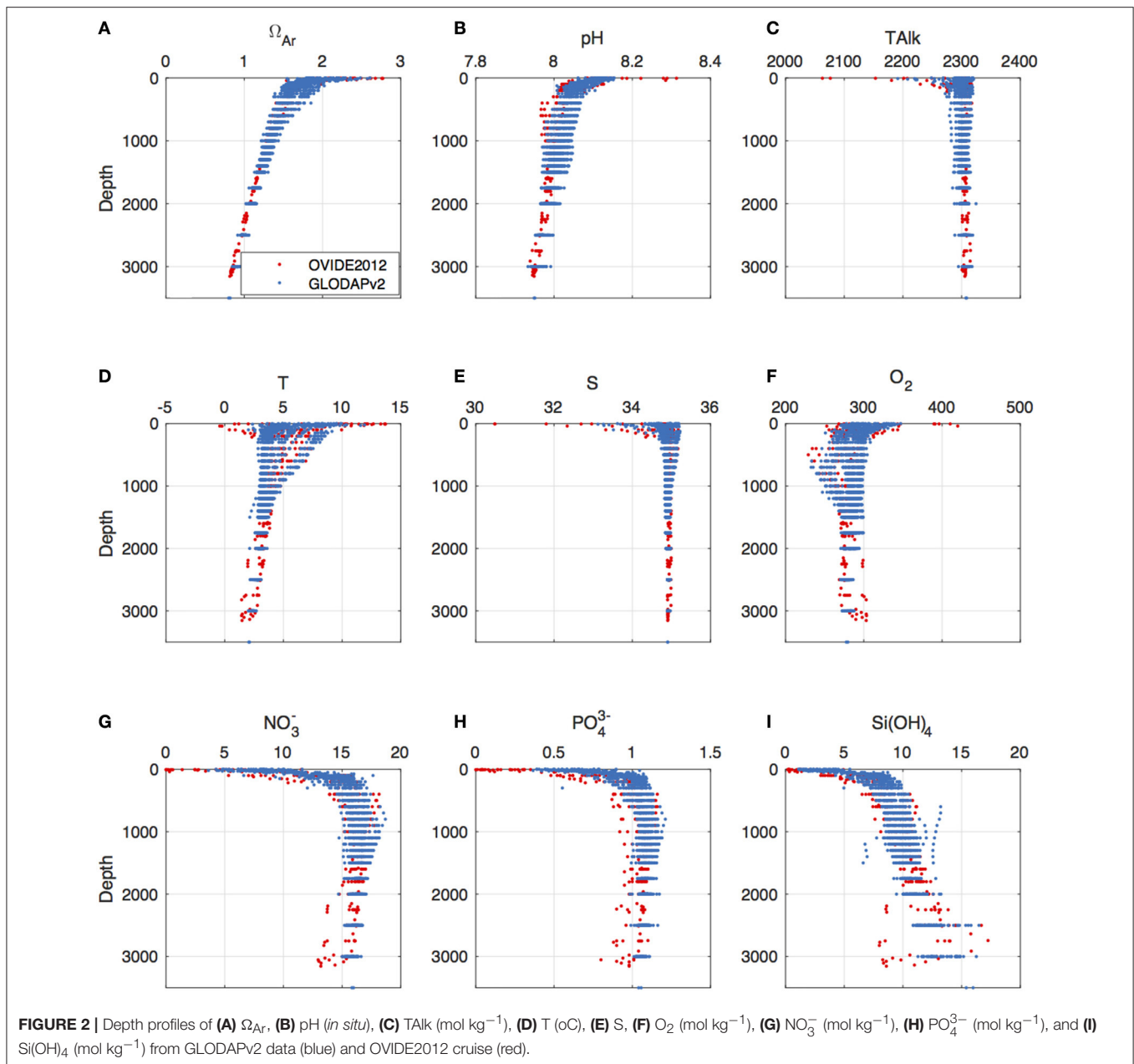
Note that a few stations from the OVIDE2012 data set fall outside of our modified Longhurst ARCT biogeochemical province boundary (Figure 1). Specifically, stations closer to Greenland where a lower Ω_{Ar} could be expected due to higher fresh water input.

RESULTS AND DISCUSSION

Depth Profiles of Variables

Depth profiles from 0 to 3,500 m from the GLODAPv2 data for all variables over the study domain, are presented in Figure 2 (blue dots). All variables show the highest variability in the upper 0–100 m, the approximate depth of the euphotic zone. This is the depth layer where photosynthesis, which acts to remove nutrients and TCO_2 and add O_2 , is taking place. Consequently, there is a sharp decrease in NO_3^- , and PO_4^{3-} and Si(OH)_4 , and increase in O_2 , pH, and Ω_{Ar} which reflects the seasonal bias in the GLODAPv2 data. In addition, the surface part of the euphotic zone (the approximate depth of 0–30 m) is also affected by local heating/cooling, freshwater inputs, and by air-sea exchange of CO_2 and O_2 . During the boreal summer, when most GLODAPv2 data is collected, the subpolar North Atlantic Sea exhibits warming and increased fresh water input due to ice melt resulting in slightly higher T and lower S in this surface part of the euphotic zone in comparison to the layer below (30–100 m). In addition, nutrients concentrations are lower and pH higher at the surface layer due to strong biological uptake.

Below the euphotic zone (>100 m), where photosynthesis is not present, respiration and remineralization of nutrients and organic matter dominates. These processes lead to a gradual increase of NO_3^- , PO_4^{3-} , and Si(OH)_4 , and lower O_2 , pH and Ω_{Ar} . T decreases in this depth layer, but S and TALK stay nearly constant. Below 1,000 m, T, pH, and Ω_{Ar} continue to decrease down to 3,500 m, while S, TALK, O_2 , NO_3^- , and PO_4^{3-} stay nearly constant. Si(OH)_4 is the only variable that increases in deep layers due mainly to the deep water masses containing a higher fraction of water from the Arctic Sea (Ragueneau et al., 2001). There is also a contribution of Si(OH)_4 from sediment sources, but this is relatively small. Ω_{Ar} shows values reaching 2.6 in the upper 100 m and decreases with depth to 0.8 at 3,500 m. The Ω_{Ar} compensation depth ($\Omega_{Ar} = 1$) is observed at about 2,300–2,500 m, which is similar to previous studies in the Labrador Sea



(2,300 m, Azetsu-Scott et al., 2010) and lower than reported in the Iceland Sea (1,710 m, Olafsson et al., 2009)

All variables from the OVIDE2012 cruise show similar range of values within the modified Longhurst ARCT biogeochemical province boundary as GLODAPv2 (Table 1). The OVIDE2012 show slightly lower T, S, and TALK due to inclusion of a few stations close to Greenland with higher freshwater content that are out of the ARCT border. OVIDE2012 data also shows lower nutrient levels values and NO₃⁻ and PO₄³⁻ depletion, while in GLODAPv2 nutrients were not depleted in the study area. This difference could be due to particular conditions during 2012, or more likely due to the bin-averaging inherent in creating the GLODAPv2 data.

Relationships between GLODAPv2 Variables

The pairwise scatter plots for the GLODAPv2 variables; Ω_{Ar} , pH (*in situ*), TALK, T, S, O₂, nutrients and P, and histograms for each of the variables are presented in Figure 3. Most of these variables and the relationships between them show variations with depth reflecting different biogeochemical regimes and the processes through the water column noted in the section on Depth Profiles of Variables. This suggests that depth is an important variable for constructing predictive algorithms. Based on examining depth profiles, we divided data into three depth layers (0–100, 100–500, 500–3,500 m) approximately reflecting the different biogeochemical regimes (euphotic zone,

respiration/remineralization zone, and deep water). The depth division also allows for better visualization to highlight major features of variable inter-relationships and how they change with depth.

TABLE 1 | Range of values between 0 and 3,500 m for all variables from GLODAPv2 and OVIDE2012 (Figure 1).

	GLODAPv2	OVIDE2012
T (°C)	2.0–11.9	−0.4–13.6
S	33.1–35.2	30.4–35.1
O ₂ (μmol kg ^{−1})	232–347	229–420
NO ₃ [−] (μmol kg ^{−1})	3.6–18.6	0–18.2
PO ₄ ^{3−} (μmol kg ^{−1})	0.36–1.21	0–1.16
Si(OH) ₄ (μmol kg ^{−1})	1.11–16.4	0.21–17.2
TALK (μmol kg ^{−1})	2,191–2,324	2,062–2,317
pH (<i>in situ</i>)	7.93–8.15*	7.93–8.31
Ω_{Ar}	0.80–2.60*	0.81–2.77*

Calculated variables are marked with *.

For individual variables, the histograms suggest non-symmetric distributions (excepting O₂), and sometimes are indicative of bi-modality (pH, T) due to the different depth regimes. Perhaps the most notable feature is the strong dependence (correlation) amongst the variables. Correlations of Ω_{Ar} with other variables (Figure 3, top panels) for the three depth layers are shown in Table 2. In the euphotic zone (0–100 m), we observe negative correlation of Ω_{Ar} with nutrients and O₂ and positive with pH reflecting biological uptake and

TABLE 2 | Correlations (*r*) of GLODAPv2 variables with Ω_{Ar} for the three depth layers.

Depth (m)	pH	TALK	T	S	NO ₃ [−]	PO ₄ ^{3−}	Si(OH) ₄	O ₂
0–100	0.49	0.60	0.78	0.51	−0.37	−0.69	−0.57	−0.48
100–500	0.45	0.64	0.74	0.39	−0.63	−0.72	−0.73	−0.39
500–3,500	0.83	−0.07	0.66	0.02	0.11	−0.01	−0.73	−0.03

Correlations >0.7 are considered strong, 0.3–0.7 moderate and <0.3 weak.

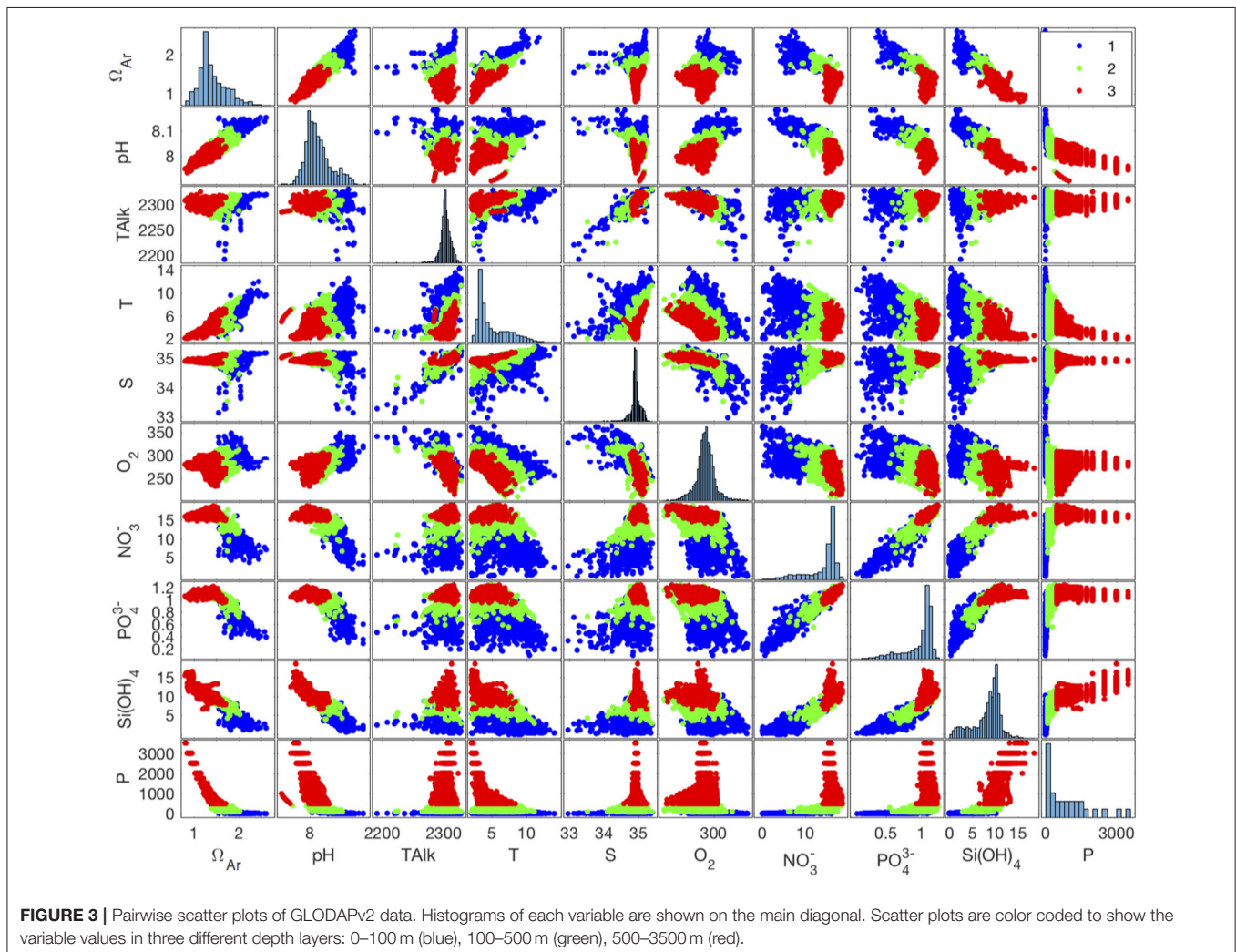


FIGURE 3 | Pairwise scatter plots of GLODAPv2 data. Histograms of each variable are shown on the main diagonal. Scatter plots are color coded to show the variable values in three different depth layers: 0–100 m (blue), 100–500 m (green), 500–3500 m (red).

photosynthesis. Positive correlations are also found with T, S (stoichiometric solubility is a function of T, S, P) and TALK (affecting CO_3^{2-}). The strongest inter-correlations in this depth layer are found with T, TALK, PO_4^{3-} , and Si(OH)_4 and moderate ones between pH, S, and O_2 and NO_3^- (Table 2). Note that the variables pH, O_2 , and NO_3^- are not included in CO_2SYS as input variables for calculating GLODAPv2 Ω_{Ar} . Correlations of similar strength and the same sign as above are found in 100–500 m layer, where photosynthesis is not present, but respiration and remineralization of nutrients and organic matter dominates. This implies similar stoichiometry of biological uptake and remineralization. Slightly stronger correlations with nutrients, in particular with NO_3^- , and weaker correlation with S are observed. In the deep layer (500–3,500 m) strong correlations are only found with variables that are changing at these depths; pH, T, and Si(OH)_4 . The relationships between measured OVIDE2012 variables are consistent with those from GLODAPv2 (not shown).

We also note that in the surface part of the euphotic zone (0–30 m), local heating/cooling, gas exchange and freshwater inputs may affect inorganic carbon and O_2 , and decouple the $\text{O}_2:\text{CO}_2$ stoichiometry. This consequently could lead to different relationships between the variables at the surface (0–30 m) than those found in the remaining of euphotic zone below (30–100 m). For this reason, some of the previous studies (Juranek et al., 2009, 2011; Alin et al., 2012) excluded 0–30 and 0–15 m from their analysis. We found that regression coefficients were similar when excluding data from 0 to 30 m data and have, therefore, based the analysis on using all data from 0 to 100 m.

Algorithm Training: Estimating Ω_{Ar} Using Observations

Unsupervised Learning: MLR Applied to Training Data All variables regression

When including all non-carbonate and autonomous sensor variables (0–3,500 m) in the model (Equation 2) the R^2 is very high (98%), and an F -test indicates that the overall regression is highly significant ($p < 10^{-15}$). T -tests also show that all individual predictors are significant, with the exception of O_2 . Figure 4 shows the R^2 from “all variables regression” for different combination of 1–8 predictor variables [T, S, P, O_2 , pH, NO_3^- , PO_4^{3-} , Si(OH)_4]. This exercise indicates how, for a given level of complexity (or number of predictors), different combinations of variables affect the fit. It also provides information as to how adding and/or removing certain predictors can change the goodness of fit, which can be useful as guidance for a selection (and development) of additional sensors for existing platforms. The results suggest T and pH is the best combination of two key explanatory variables, which together can explain 95 % of variability in Ω_{Ar} , followed by a combination of P and PO_4^{3-} ($R^2 = 0.94$). The best combination of three predictors are T, P, and PO_4^{3-} ($R^2 = 0.96$), closely followed by T, pH, and NO_3^- , and the best four predictors are T, P, pH, and PO_4^{3-} ($R^2 = 0.98$). The all variables regression suggests that T, P, pH, and PO_4^{3-} are the most important predictors for Ω_{Ar} , although differences in R^2 are quite small.

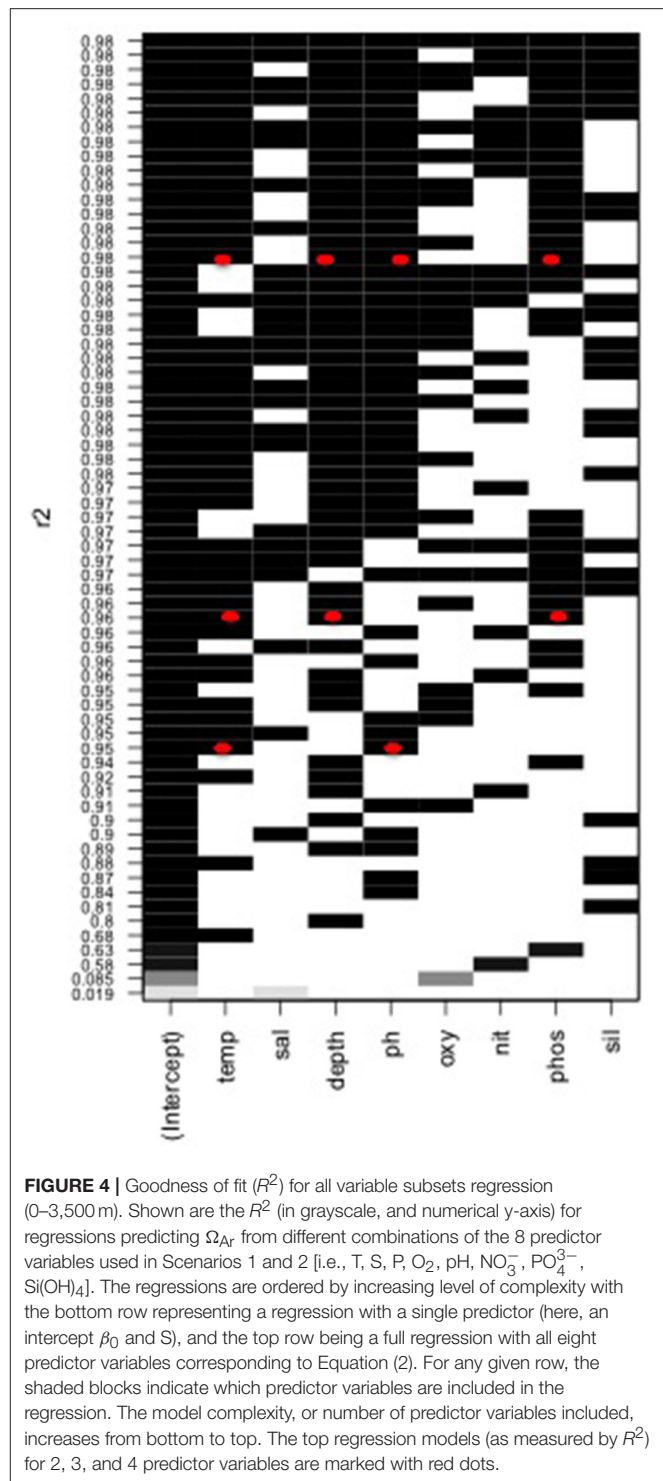


FIGURE 4 | Goodness of fit (R^2) for all variable subsets regression (0–3,500 m). Shown are the R^2 (in grayscale, and numerical y-axis) for regressions predicting Ω_{Ar} from different combinations of the 8 predictor variables used in Scenarios 1 and 2 [i.e., T, S, P, O_2 , pH, NO_3^- , PO_4^{3-} , Si(OH)_4]. The regressions are ordered by increasing level of complexity with the bottom row representing a regression with a single predictor (here, an intercept β_0 and S), and the top row being a full regression with all eight predictor variables corresponding to Equation (2). For any given row, the shaded blocks indicate which predictor variables are included in the regression. The model complexity, or number of predictor variables included, increases from bottom to top. The top regression models (as measured by R^2) for 2, 3, and 4 predictor variables are marked with red dots.

Stepwise regression

In all cases, the best regression model chosen by the various variable selection procedures (forward selection, backward elimination, and forward/backward combination) eliminated only the O_2 variable, with the final chosen model therefore being a regression of the response variable Ω_{Ar} on T, S, P, pH, NO_3^- ,

PO_4^{3-} , Si(OH)_4 . It is likely that O_2 is eliminated by the selection procedures due to its relatively low correlation with Ω_{Ar} (Table 1) as well as its strong relationship with other predictor variables (Figure 3).

Supervised Learning: MLR Regression Scenarios

Table 3 gives a summary of the regression statistics based on GLODAPv2 data from 0 to 3,500 m for the three scenarios described in section Multiple Linear Regression (MLR) Algorithms (Training). We define the algorithm provides a “good” estimate of Ω_{Ar} when $R^2 > 0.98$ and $\text{RMSE} < 0.05$ (i.e., uncertainty in GLODAPv2 Ω_{Ar}) and an “adequate” estimate when $R^2 > 0.95$ and RMSE is smaller than 2x uncertainty in GLODAPv2 Ω_{Ar} (0.1).

Scenario 1—non-carbonate

T and S alone are not “adequate” predictors of Ω_{Ar} , ($R^2 = 0.822$, $\text{RMSE} = 0.153$, not shown in Table 3). Inclusion of depth dependence through P improves the R^2 and RMSE , confirming depth is important predictor, but still does not yield an “adequate” estimate of Ω_{Ar} . The combination of T, S, NO_3^- , and P can “adequately” predict the Ω_{Ar} variable. PO_4^{3-} is slightly better predictor than NO_3^- , and the combination of T, S, P, NO_3^- , and PO_4^{3-} yields $R^2 = 0.969$, $\text{RMSE} = 0.064$ (not shown in Table 3). The addition of Si(OH)_4 , does not significantly improve prediction. As with the “all variables regression,” this suggests that PO_4^{3-} is the most important predictor nutrient in our study domain.

Scenario 2—autonomous sensors

Our results suggest that autonomous sensor measurements of T, S, P, and O_2 can provide “adequate” predictability of Ω_{Ar} for our study domain. Nitrate provides similar information as oxygen, while inclusions of pH improves predictability by a small amount suggesting it may be useful to add pH sensors on autonomous floats like Argo and moorings (K1, OSNAP, etc.). We also tested the use of apparent oxygen utilization (AOU), the difference between the measured O_2 concentration and its equilibrium saturation concentration, as a predictor variable instead of O_2 . AOU is known to be a better metric for biological activity than O_2 , but using AOU as a predictor variable did not improve the regression.

Scenario 3— CO_2SYS

The multiple regression model with input corresponding to the CO_2SYS input variables, yields “good” predictability ($R^2 = 0.985$, $\text{RMSE} = 0.044$). This is better than achieved in Scenario 1 and 2. This is an extremely good fit in terms for a linear regression model based on bin-averaged bottle data. The implication is that there is essentially a linear relation between Ω_{Ar} and the CO_2SYS inputs at least within the range of variations in the variable levels found within the study domain.

For simplicity, we focused mainly on the statistics of the least-squares regression fit and mostly avoided statistical inference (significance testing and p -values). Note that residuals plots however, were examined during model fitting and it was found that regression assumptions were mostly satisfied,

TABLE 3 | Regression fit (R^2) and root mean squared error (RSME), and regression coefficient \pm standard error (SE) for different combination of non-carbonate, autonomous sensors and CO_2SYS variables from the GLODAPv2 data from 0 to 3,500 m ($n = 1,631$).

Scenario/ variables	R^2	RSME	Coefficient \pm SE
NON-CARBONATE			
T, S, P	0.938	0.090	$\beta_0 = 12.3310 \pm 0.4978$ $\beta_1 = 0.1087 \pm 0.0018$ $\beta_2 = -0.3199 \pm 0.0144$ $\beta_3 = -0.2017\text{e-}03 \pm 3.6473\text{e-}06$
T, S, NO_3^- , P	0.959	0.073	$\beta_0 = -2.1368 \pm 0.6388$ $\beta_1 = 0.0465 \pm 0.0025$ $\beta_2 = 0.1194 \pm 0.0905$ $\beta_3 = -0.03768 \pm 0.00128$ $\beta_4 = -0.2315\text{e-}03 \pm 3.128\text{e-}06$
T, S, NO_3^- , PO_4^{3-} , Si(OH)_4 , P	0.969	0.063	$\beta_0 = -1.1479 \pm 0.5607$ $\beta_1 = 0.0392 \pm 0.0022$ $\beta_2 = 0.0980 \pm 0.0166$ $\beta_3 = -0.0047 \pm 0.0022$ $\beta_4 = -0.7703 \pm 0.0351$ $\beta_5 = 0.0092 \pm 0.0020$ $\beta_6 = -0.2451\text{e-}03 \pm 3.9485\text{e-}06$
AUTONOMOUS SENSORS			
T, S, O_2 , P*	0.957	0.075	$\beta_0 = 2.8475 \pm 0.5438$ $\beta_1 = 0.1156 \pm 0.00155$ $\beta_2 = -0.0861 \pm 0.0148$ $\beta_3 = 4.4712\text{e-}03 \pm 0.1659\text{e-}03$ $\beta_4 = -0.1774\text{e-}03 \pm 3.1687\text{e-}06$
T, S, O_2 , pH, P	0.978	0.054	$\beta_0 = -25.800 \pm 0.826$ $\beta_1 = 0.0750 \pm 0.0015$ $\beta_2 = 0.0212 \pm 0.0109$ $\beta_3 = 4.5133\text{e-}04 \pm 1.5595\text{e-}04$ $\beta_4 = 3.2579 \pm 0.0828$ $\beta_5 = -0.1042\text{e-}03 \pm 2.9201\text{e-}06$
T, S, O_2 , pH, NO_3^- , P	0.978	0.053	$\beta_0 = -25.819 \pm 0.8255$ $\beta_1 = 0.0701 \pm 0.0031$ $\beta_2 = 0.0387 \pm 0.0147$ $\beta_3 = 2.0956\text{e-}04 \pm 2.0922\text{e-}04$ $\beta_4 = 3.2013 \pm 0.0886$ $\beta_5 = -3.0580\text{e-}03 \pm 1.7460\text{e-}03$ $\beta_6 = -0.1095\text{e-}03 \pm 4.2277\text{e-}06$
CO_2SYS			
T, S, TALK, pH, PO_4^{3-} , Si(OH)_4 , P	0.985	0.044	$\beta_0 = -21.4630 \pm 0.6870$ $\beta_1 = 0.0488 \pm 0.0016$ $\beta_2 = -0.0749 \pm 0.0146$ $\beta_3 = 3.6093\text{e-}03 \pm 2.3167\text{e-}03$ $\beta_4 = 2.1860 \pm 0.0780$ $\beta_5 = -0.4874 \pm 0.0205$ $\beta_6 = 0.0125 \pm 0.0013$ $\beta_7 = -0.1777\text{e-}03 \pm 3.6385\text{e-}06$

These cases are used for validation in section Validation: Testing the Ω_{Ar} Algorithms Using Independent Ship Data, case marked with * is used for application to K1 mooring time series.

excepting the violation of non-constant variance in some cases. This would normally be corrected by transformation, but such transformation would be case-specific and make

algorithm comparison more difficult but is recommended when developing a targeted algorithm. Similarly, no attempts were made to include interaction terms or polynomial terms when building regression models. Our experience showed that little was to be gained from the addition of such complexity, and such models also suffer from difficulty in interpretation and

exacerbate the effects of multicollinearity on the regression. The multicollinearity in the predictor variables is a ubiquitous feature in oceanographic problems and a consequence of a myriad of interacting physical-chemical processes, which dynamically link the variables. While complicating the interpretation of the statistical analysis, a positive effect of this variable dependence

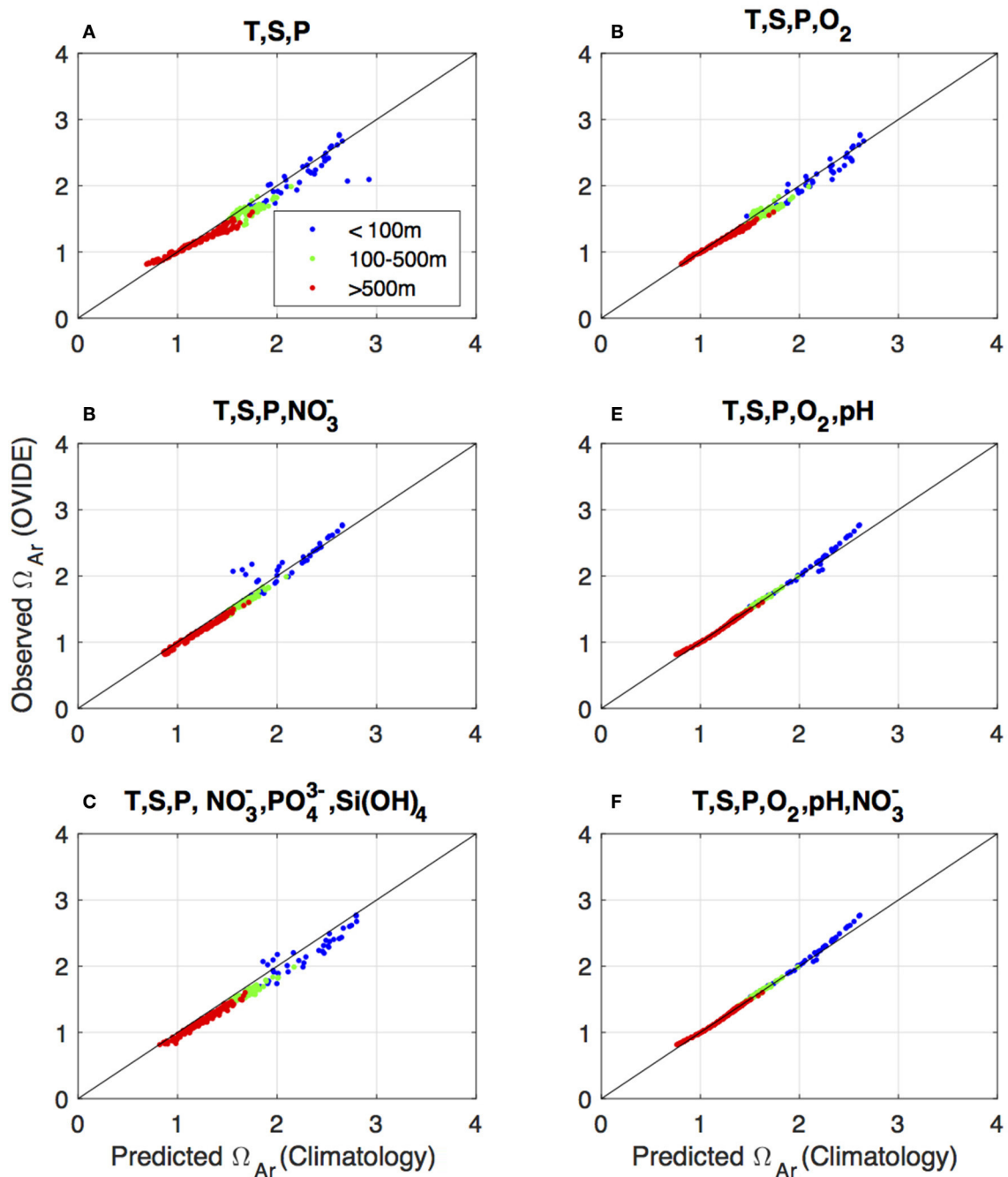


FIGURE 5 | Validation plots of estimated Ω_{Ar} from empirical algorithms vs. observed Ω_{Ar} from OVIDE2012 cruise. These are done for different selections of non-carbonate (A–C) variables and autonomous sensor (D–F) variables. Observed refers to Ω_{Ar} calculated from OVIDE2012 pH and TALK. The 1:1 line is shown in black.

is that there is considerable flexibility in choosing predictor variables for empirical algorithms (i.e., the trading of ease of measurement vs. predictive skill).

Validation: Testing the Ω_{Ar} Algorithms Using Independent Ship Data

In this section, we assess how well the non-carbonate and autonomous sensor empirical algorithms, which were trained using the GLODAPv2 data normalized to 2002, are able to predict Ω_{Ar} for an independent data set, the OVIDE2012 cruise. Validation plots and corresponding quantitative metrics for the selected algorithms (Table 3) are presented in Figure 5 and Table 4. Overall, the validation plots in Figure 5 indicate a very good correspondence between the observed and predicted Ω_{Ar} . In all cases, the points cluster tightly near the 1:1 line indicating little bias and a small level of variability. The overall results in Table 4 also indicate successful validation with: (i) a correlation close to one, (ii) a consistently good fit (low RMSE), (iii) a small bias (AAE), but one that is slightly positive (AE), (iv) observations that differ from predictions by a factor close to

one (RI); and (v) a model with consistent predictive skill (MEF between 0.5 and 1). Specific cases are discussed below.

Scenario 1 – Non-Carbonate

For the non-carbonate scenario (Figures 5A–C, Table 4), the physical case (T, S, P) has the worst fit, particularly for the two shallowest depth layer (0–100 and 0–500 m) where oceanographic variability is highest. The addition of nitrate (the T, S, NO_3^- , P case) reduces the variability (r , RMSE) and bias (AE). Inclusion of the full nutrient suite [the T, S, P, NO_3^- , PO_4^{3-} , and Si(OH)_4 case] yields slightly degraded performance with increased bias.

Scenario 2 – Autonomous Sensors

All three algorithms with autonomous sensors variables (Figures 5D–F, Table 4) have consistently good and quite similar overall predictability over the full water depth (0–3,500 m). The T, S, O_2 , P algorithm has good performance in the deep layer (500–3,500 m) and may be sufficient for the prediction of Ω_{Ar} there, but has the lowest performance in the 0–100 and

TABLE 4 | Quantitative validation metrics: correlation (r), root mean squared error (RMSE), the reliability index (RI), the average error (AE), the average absolute error (AAE), and the modeling efficiency (MEF), all calculated according to Stow et al. (2009), for comparison of predicted Ω_{Ar} (Equation 2, with regression coefficients given in Table 3) with Ω_{Ar} calculated from observed TALK and pH using CO_2SYS ($n = 303$).

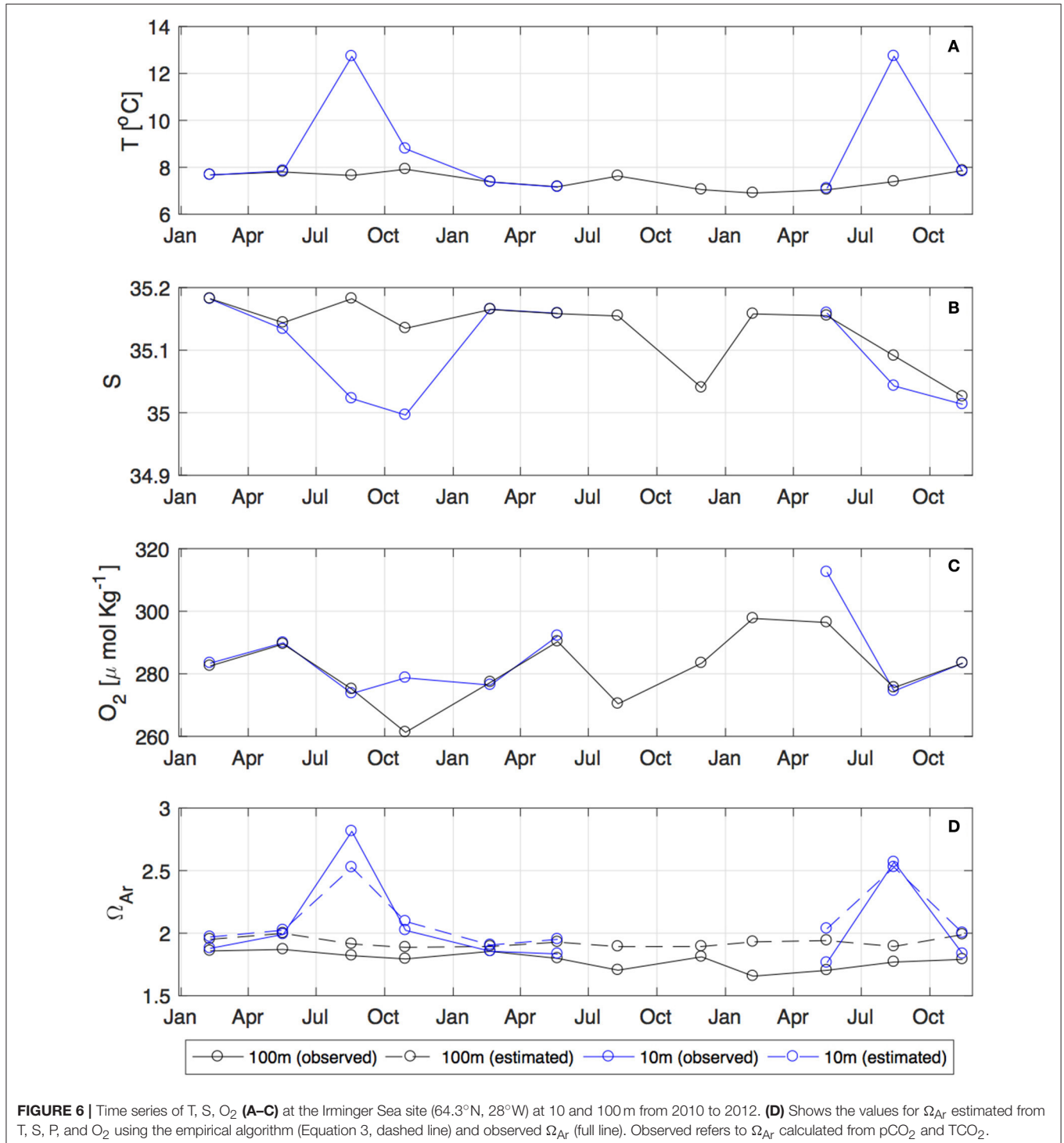
Scenario/variables	Depth (m)	r	RSME	AE	AAE	RI	MEF
NON-CARBONATE							
T, S, P	0–3,500	0.975	0.113	0.064	0.082	1.073	0.914
	0–100	0.865	0.195	0.087	0.124	1.088	0.667
	100–500	0.801	0.113	0.082	0.088	1.069	–0.234
	500–3,500	0.984	0.087	0.054	0.071	1.071	0.740
T, S, NO_3^- , P	0–3,500	0.984	0.083	0.047	0.066	1.056	0.953
	0–100	0.902	0.153	–0.039	0.100	1.084	0.795
	100–500	0.970	0.072	0.067	0.067	1.045	0.493
	500–3,500	0.994	0.064	0.059	0.059	1.053	0.857
T, S, NO_3^- , PO_4^{3-} , Si(OH)_4 , P	0–3,500	0.992	0.103	0.088	0.093	1.070	0.929
	0–100	0.947	0.157	0.110	0.142	1.076	0.783
	100–500	0.948	0.116	0.109	0.109	1.071	–0.305
	500–3,500	0.990	0.081	0.076	0.076	1.068	0.774
AUTONOMOUS SENSORS							
T, S, O_2 , P	0–3,500	0.991	0.067	0.042	0.055	1.042	0.969
	0–100	0.962	0.102	0.044	0.086	1.049	0.908
	100–500	0.890	0.081	0.058	0.074	1.049	0.359
	500–3,500	0.996	0.050	0.036	0.040	1.038	0.913
T, S, O_2 , pH, P	0–3,500	0.997	0.029	–0.004	0.018	1.018	0.994
	0–100	0.989	0.064	–0.030	0.047	1.027	0.963
	100–500	0.993	0.016	–0.010	0.013	1.010	0.974
	500–3,500	0.996	0.017	0.004	0.014	1.018	0.989
T, S, pH, O_2 , NO_3^- , P	0–3,500	0.998	0.027	–0.003	0.018	1.017	0.995
	0–100	0.994	0.060	–0.036	0.044	1.025	0.968
	100–500	0.994	0.014	–0.008	0.012	1.009	0.980
	500–3,500	0.996	0.017	0.006	0.014	1.017	0.989

0–500 m depth layer. The addition of pH in the 0–100 and 0–500 m provides an improvement, while little incremental improvement is achieved from the addition of NO_3^- . The algorithms that include pH have small negative bias in the upper two layers (0–100 and 0–500 m). The validation using OVIDE2012 pH corrected for the decadal decrease reported for Irminger Sea of -0.025 slightly increased the bias. The

good predictability implies that the algorithms are insensitive to decadal anthropogenic changes in the carbonate system.

Application

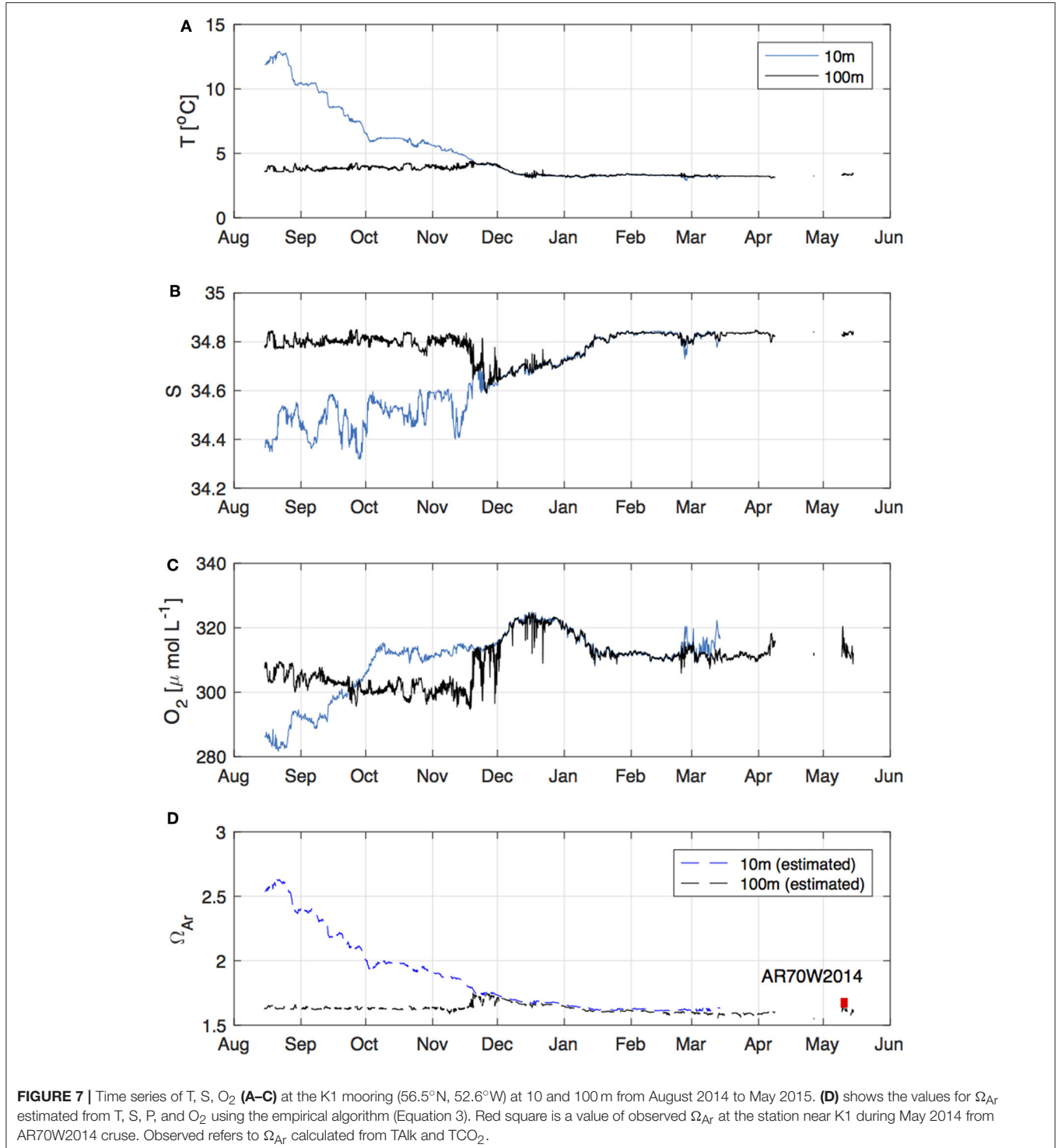
Empirical algorithms trained on GLODAPv2 data (see **Table 3**) were applied to time series of T, S, O_2 , and P at 10 and 100 m to estimate Ω_{Ar} at two sites: (1) Irminger Sea during 2010–2012



(Figures 6A–D, P not shown) and (2) K1 mooring in Labrador Sea during August 2014 to March 2015 (Figures 7A–D, P not shown). The regression equation used for this application is (see also Table 3):

$$\Omega_{Ar} = 2.8475 + 0.1156 T - 0.0861 S + 4.4712e-03 O_2 - 0.1774e-03 P \quad (4)$$

At Irminger Sea site, we compared the estimated Ω_{Ar} using Equation (4) to Ω_{Ar} calculated from observations of TCO₂ and pCO₂ using CO₂SYS (Figure 6D). Calculated Ω_{Ar} showed good agreement with estimated values at both 10 and 100 m. Observations of inorganic carbon variables at K1 mooring location during our time-series observations were not available for comparison. To attempt to assess the validity of estimated



Ω_{Ar} (Figure 7D), we compared our values to the Ω_{Ar} calculated from observations of TCO₂ and TALK at the station near the K1 mooring that have been collected on yearly spring (May/June) AR07W cruises since 1998 (https://www.nodc.noaa.gov/ocads/oceans/RepeatSections/clivar_ar07w.html). Consistent with our observations, Ω_{Ar} from 1998 to 2014 showed higher values at 10 m compared to 100 m. Large interannual variability was observed with Ω_{Ar} ranging between 2.7 and 1.5 at 10 m and between 2.0 and 1.5 at 100 m. Ω_{Ar} at both depths showed a decreasing trend. In May 2014, Ω_{Ar} measured on AR07W2014 cruise (Yashayaev and Azetsu-Scott, 2016) showed values 1.72 at 10 m and 1.67 at 100 m, and decreasing to 0.8 at 3,500 m. This is consistent to what would be expected for Ω_{Ar} , based on our algorithm (Equation 4). However direct comparison is not possible since the K1 mooring data was not available in May 2014. We further compared our Ω_{Ar} to the literature values in the Labrador Sea (Azetsu-Scott et al., 2010) and Ω_{Ar} calculated from pH and TALK on Redfish cruises (June/July 2013, unpublished data) from the region west from the K1 mooring. Both show summer values of Ω_{Ar} around 2.4, consistent with our estimates. Our observation emphasize the need for pH sensors on moorings in the area.

As expected, estimated Ω_{Ar} at 10 m depth exhibits seasonal variability at both sites, Irminger Sea and K1 mooring, with highest values in August (around 2.5) due to biological

drawdown of inorganic carbon during the summer. Ω_{Ar} then gradually decreased and showed lowest values at Irminger in February (around 1.9). At the K1 mooring Ω_{Ar} decreased to 1.5–1.6 in December, and continued to stay at this value through the winter. At 100 m, estimated Ω_{Ar} remained at values between 1.9 and 2.0 at Irminger site, and 1.5 and 1.7 at K1 mooring without seasonal variation, which indicates biological uptake at this depth was negligible. Similar values of Ω_{Ar} at 10 and 100 m during the winter are expected due to mixing of surface water down to various depths during convection in the area, which results in fairly uniform Ω_{Ar} values over the convection depth (Azetsu-Scott et al., 2010). During winter of 2014, an extreme convection event occurred and extended to about 1,700 m (Yashayaev and Loder, 2016), so presumably the surface values of Ω_{Ar} from K1 mooring could be representative of the water column down to that depth.

We have also applied empirical algorithms from previous studies that used T, S, O₂, and P or T, O₂, and P to predict Ω_{Ar} along the central Oregon coast (Juraneck et al., 2009; Figure 8, red line) and in the Sea of Japan (Kim et al., 2010; Figure 7, black lines). These algorithms either under-predict or over-predict the known values of Ω_{Ar} in our study domain by a significant amount (more than 0.5). This confirms the need for development of regionally specific algorithms. A caveat of our approach is the use of seasonally biased (mainly summer) climatological

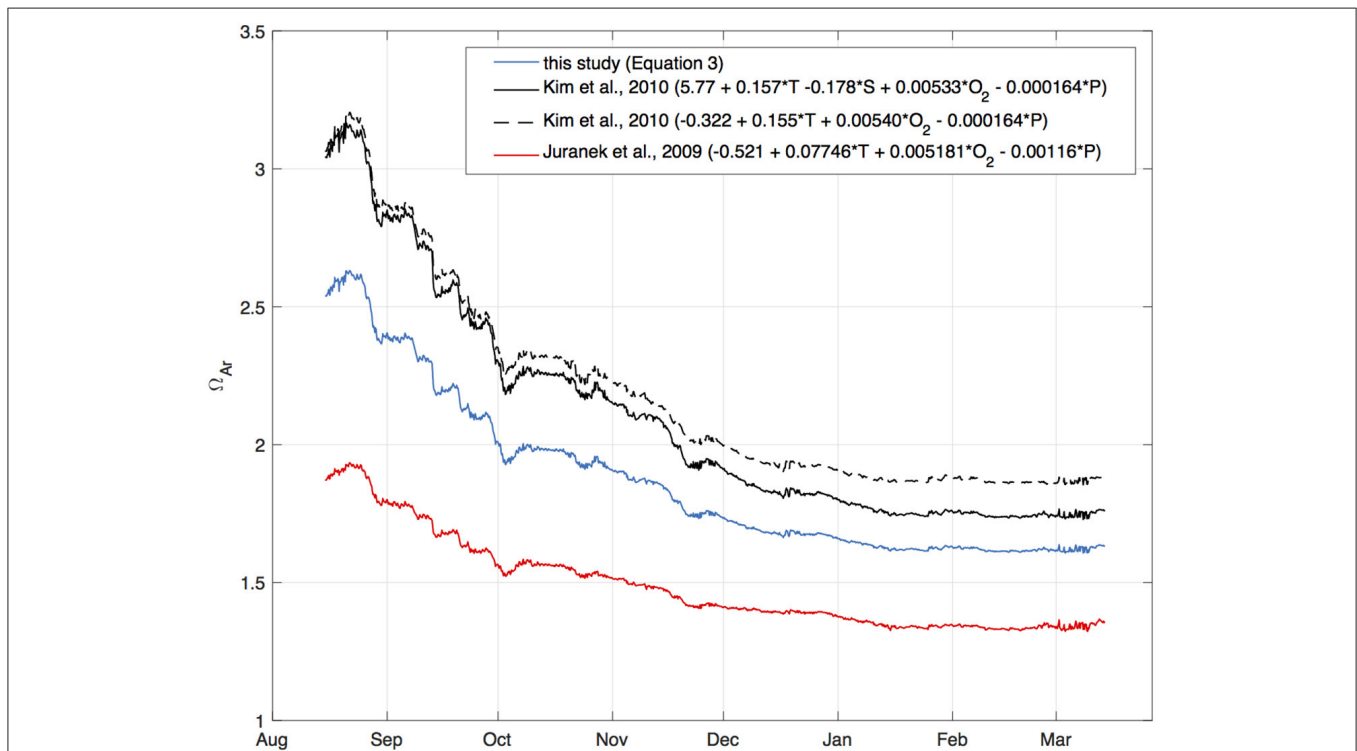


FIGURE 8 | Ω_{Ar} estimated from time series of T, S, O₂, and P (or T, O₂, and P) at the K1 mooring (56.5°N, 52.6°W) at 10 m depth from August 2014 to March 2015 using three different empirical algorithms from: (a) this study, Equation 4 (blue line), (b) central Oregon coast (Juraneck et al., 2009) (red line), and (c) the Sea of Japan (Kim et al., 2010) (black lines).

data to train the algorithms and summer ship data to validate them.

CONCLUSIONS

Our study suggests that linear regression models (empirical algorithms) based on the GLODAPv2 data bin-averaged in $1^\circ \times 1^\circ$ cells can successfully be used to estimate Ω_{Ar} in the North Atlantic Subpolar region. Another key feature is in producing reliable error bounds for any estimates of Ω_{Ar} . Algorithms based on non-carbonate variables indicate that Ω_{Ar} can be predicted well from entirely non-carbonate observations, with PO_4^{3-} being the best nutrient predictor. Algorithms using autonomous sensor variables emphasize the importance of adding pH sensors on autonomous floats like Argo and moorings (K1, OSNAP, etc.), in particular in the euphotic and remineralization zone. In deeper water, observations of T, S, and O_2 may be sufficient for predicting Ω_{Ar} . Different regression model building strategies suggest PO_4^{3-} measurements are desirable. It appears that there is essentially a linear relation between Ω_{Ar} and the CO_2SYS input variables at least within the range of variations in the variable levels found here.

Validation with independent ship data showed good correspondence, with small bias and variability. Since the anthropogenic trend in Ω_{Ar} has been removed, the algorithms have no temporal component to them (i.e., no time variable as predictor). Nevertheless, the validation with OVIDE2012 data show that the algorithms trained on 2002 data manage to successfully estimate Ω_{Ar} in 2012. This shows the robustness of the algorithms to changes over a short time interval (such as a decade).

The empirical algorithms also performed well even though they are being applied outside the range of values used to train the algorithms. This suggests that, while they are regional algorithms, they may have much broader spatial applicability. Future work seeks to identify appropriate biogeochemical provinces for which a regional algorithm is valid. Since the relationship of variables with Ω_{Ar} may be correlative, rather than directly causal, emphasis must be on validating predictive skill using independent data.

REFERENCES

- Alin, S. R., Feely, R. A., Dickson, A. G., Hernández-Ayón, J. M., Juraneck, L. W., Ohman, M. D., et al. (2012). Robust empirical relationships for estimating the carbonate system in the southern California Current System and application to CalCOFI hydrographic cruise data (2005–2011). *J. Geophys. Res.* 117:C05033. doi: 10.1029/2011JC007511
- Allen, J.I., Holt, J. T., Blackford, J., and Proctor, R. (2007). Error quantification of a high-resolution coupled hydrodynamic-ecosystem coastal-ocean model: part 2. Chlorophyll-a, nutrients and SPM. *J. Mar. Syst.* 68, 381–404. doi: 10.1016/j.jmarsys.2007.01.005
- Azetsu-Scott, K., Clarke, A., Falkner, K., Hamilton, J., Jones, E. P., Lee, C., et al. (2010). Calcium carbonate saturation states in the waters of the Canadian Arctic Archipelago and the Labrador Sea. *J. Geophys. Res.* 115:C11021. doi: 10.1029/2009JC005917

Application to Station K1 time series, as well as time series from the Irminger Sea suggest the potential for regionally tuned algorithms, but they need to validate against measured Ω_{Ar} to properly assess their performance. Finally, algorithms require evolution and recalibration by ongoing periodic carbon-dedicated cruises in order to account for secular trends in anthropogenic CO_2 .

AUTHOR CONTRIBUTIONS

DT: Lead the research and writing of the manuscript; MD: Contributed to analysis of the data and writing of the paper; SKL: Provided guidance with GLODAPv2 data and contributed to writing of the paper; JK: Provided mooring data and comments; FA-P and FP: Collected and analyzed shipboard data and provided comments. All authors contributed to proofing of the manuscript.

FUNDING

MD was supported by an NSERC Discovery Grant, and SKL was supported by the EU H2020 research and innovation project AtlantOS (grant agreement no 633211). The OVIDE-12 cruise and the contribution of FA-P and FP were supported by the Spanish Ministry of Economy and Competitiveness through the project CTM2013-41048-P co-funded by the Fondo Europeo de Desarrollo Regional 2014-2020 (FEDER). K1 mooring is an Oceansites site supported by the EU Horizon 2020 research and innovation program AtlantOS (grant agreement no 633211). LDEO contribution no 8169.

ACKNOWLEDGMENTS

We are grateful to D.W.R. Wallace and CERC.OCEAN, and S. Gulev for their contributions at the initial stages of this study, and J. Olafsson, and S.R. Olafsdottir for making the Irminger Sea site data publicly available. We thank the editor and two reviewers whose comments greatly helped to improve this manuscript.

- Barbero, L., Boutin, J., Merlivat, L., Martin, N., Takahashi, T., Sutherland, S., et al. (2011). Importance of water mass formation regions for the air-sea CO_2 flux estimate in the Southern Ocean. *Glob. Biogeochem. Cycles* 25:GB1005. doi: 10.1029/2010GB003818
- Bates, N. R., Astor, Y. M., Church, M. J., Currie, K., Dore, J. E., González-Dávila, M., et al. (2014). A time-series view of changing ocean chemistry due to ocean uptake of anthropogenic CO_2 and ocean acidification. *Oceanography* 27, 126–141. doi: 10.5670/oceanog.2014.16
- Bostock, H. C., Mikaloff Fletcher, S., E., and Williams, M. J. M. (2013). Estimating carbonate parameters from hydrographic data for the intermediate and deep waters of the Southern Hemisphere oceans. *Biogeosciences* 10, 6199–6213. doi: 10.5194/bg-10-6199-2013
- Box, G. E. P., Jenkins, G. M., and Reinsel, G. C. (1994). *Time Series Analysis: Forecasting and Control*, 3rd Edn. Englewood Cliffs, NJ: Prentice Hall.
- Carter, B. R., Feely, R. A., Mecking, S., Cross, J. N., Macdonald, A. M., Siedlecki, S. A., et al. (2017). Two decades of Pacific anthropogenic carbon

- storage and ocean acidification along Global ocean ship-based hydrographic investigations program sections P16 and P02. *Glob. Biogeochem. Cycles* 31, 306–327. doi: 10.1002/2016GB005485
- Clayton, T. D., and Byrne, R. H. (1993). Spectrophotometric seawater pH measurements: total hydrogen ion concentration scale calibration of m-cresol purple and at-sea results. *Deep Sea Res. I* 40, 2115–2129. doi: 10.1016/0967-0637(93)90048-8
- DeGrandpre, M. D., Körtzinger, A., Send, U., Wallace, D. W. R., and Bellerby, R. G. J. (2006). Uptake and sequestration of atmospheric CO₂ in the Labrador Sea deep convection region. *Geophys. Res. Lett.* 33:L21S03. doi: 10.1029/2006GL026881
- Dickson, A. (1990). Standard potential of the reaction: AgCl (s) + 1/2H₂(g) = Ag (s) + HCl (aq), and the standard acidity constant of the ion HSO⁻⁴ in synthetic sea water from 273.15 to 318.15 K. *J. Chem. Thermodyn.* 22, 113–127. doi: 10.1016/0021-9614(90)90074-Z
- Dickson, A. G., Sabine, C. L., and Christian, J. R. (2007). *Guide to Best Practices for Ocean CO₂ Measurements*. PICES Spec. Publ., 3. Sidney, BC: North Pacific Marine Science Organization, p. 191.
- Fröb, F., Olsen, A., Pérez, F. F., García-Ibáñez, M. I., Jeansson, E., Omar, A., et al. (accepted). Inorganic carbon and water masses in the Irminger Sea since 1991. *Biogeosci. Discuss.* doi: 10.5194/bg-2017-27
- García-Ibáñez, M. I., Zunino, P., Fröb, F., Carracedo, L. I., Ríos, A. F., Mercier, H., et al. (2016). Ocean acidification in the subpolar North Atlantic: rates and mechanisms controlling pH changes. *Biogeosciences* 13, 3701–3715. doi: 10.5194/bg-13-3701-2016
- Hall, T. M., Haine, T. W. N., and Waugh, D. W. (2002). Inferring the concentration of anthropogenic carbon in the ocean from tracers. *Glob. Biogeochem. Cycles* 16:1131. doi: 10.1029/2001gb001835
- Hastie, T., Tibshirani, R., and Friedman, J. (2009). *The Elements of Statistical Learning*. New York, NY: Springer-Verlag.
- IPCC (2013). “Climate change 2013: the physical science basis,” in *Contribution of Working Group I to the Fifth Assessment Report of the Intergovernmental Panel on Climate Change*, eds T. F. Stocker, D. Qin, G. K. Plattner, M., Tignor, S. K. Allen, J. Boschung, A. Nauels, Y. Xia, V. Bex, and P. M. Midgley (Cambridge; New York, NY: Cambridge University Press), 1535.
- Jackson, L. C., Peterson, K. A., Roberts, C. D., and Wood, R. A. (2016). Recent slowing of Atlantic overturning circulation as a recovery from earlier strengthening. *Nat. Geosci.* 9, 518–522. doi: 10.1038/ngeo2715
- Juraneck, L. W., Feely, R. A., Gilbert, D., Freeland, H., and Miller, L. A. (2011). Real-time estimation of pH and aragonite saturation state from Argo profiling floats: prospects for an autonomous carbon observing strategy. *Geophys. Res. Lett.* 38:L17603. doi: 10.1029/2011GL048580
- Juraneck, L. W., Feely, R. A., Peterson, W. T., Alin, S. R., Hales, B., Lee, K. et al. (2009). A novel method for determination of aragonite saturation state on the continental shelf of central Oregon using multi-parameter relationships with hydrographic data. *Geophys. Res. Lett.* 36:L24601. doi: 10.1029/2009GL040778
- Kim, T.-W., Lee, K., Feely, R. A., Sabine, C. L., Chen, C. T. A., Jeong, H., et al. (2010). Prediction of Sea of Japan (East Sea) acidification over the past 40 years using a multiparameter regression model. *Glob. Biogeochem. Cycles* 24:GB3005. doi: 10.1029/2009GB003637
- Koelling, J., Wallace, D. W. R., Send, U., and Karstensen, J. (2017). Intense oceanic uptake of oxygen during 2014–2015 winter convection in the Labrador Sea. *Geophys. Res. Lett.* 44, 7855–7864. doi: 10.1002/2017GL073933
- Lauvset, S. K., Key, R. M., Olsen, A., van Heuven, S., Velo, A., Lin, X., et al. (2016). A new global interior ocean mapped climatology: the 1°x1° GLODAP version 2. *Earth Syst. Sci. Data* 8, 325–340. doi: 10.5194/essd-8-325-2016
- Lee, K., Tong, L. T., Millero, F. J., Sabine, C. L., Dickson, A. G., Goyet, C., et al. (2006). Global relationships of total alkalinity with salinity and temperature in surface waters of the world's oceans. *Geophys. Res. Lett.* 33:L19605. doi: 10.1029/2006GL027207
- Lewis, E., and Wallace, D. W. R. (1998). *Program Developed for CO₂ System Calculations*. ORNL/CDIAC-105, Carbon Dioxide Information Analysis Center, Oak Ridge National Laboratory, US Department of Energy, Oak Ridge, TN.
- Longhurst, A. (1995). Seasonal cycles of pelagic production and consumption. *Prog. Oceanogr.* 36, 77–167. doi: 10.1016/0079-6611(95)00015-1
- Lueker, T. J., Dickson, A. G., and Keeling, C. D. (2000). Ocean pCO₂ calculated from dissolved inorganic carbon, alkalinity, and equations for K-1 and K-2: validation based on laboratory measurements of CO₂ in gas and seawater at equilibrium. *Mar. Chem.* 70, 105–119. doi: 10.1016/S0304-4203(00)00022-0
- Mintrop, L., Pérez, F. F., González-Dávila, M., Santana-Casiano, J. M., and Körtzinger, A. (2000). Alkalinity determination by potentiometry: intercalibration using three different methods. *Cienc. Mar.* 26, 23–37. doi: 10.7773/cm.v26i1.573
- Montgomery, D. C., Peck, E. A., and Vining, G. G. (2015). *Introduction to Linear Regression Analysis*. Hoboken, NJ: John Wiley & Sons Inc.
- Nondal, G., Bellerby, R. G. J., Olsen, A., Johannessen, T., and Olafsson, J. (2009). Optimal evaluation of the surface ocean CO₂ system in the northern North Atlantic using data from voluntary observing ships. *Limnol. Oceanogr. Methods* 7, 109–118. doi: 10.4319/lom.2009.7.109
- Olafsson, J. (2016). *Partial Pressure (Or Fugacity) of Carbon Dioxide, Dissolved Inorganic Carbon, Temperature, Salinity and Other Variables Collected from Discrete Sample and Profile Observations Using CTD, Bottle and Other Instruments from ARNI FRIDRIKSSON and BJARNI SAEMUNDSSON in the North Atlantic Ocean from 1983-03-05 to 2013-11-13 (NCEI Accession 0149098)*. Version 1.1. NOAA National Centers for Environmental Information. Dataset.
- Olafsson, J., Olafsdottir, S. R., Benoit-Cattin, A., and Takahashi, T. (2009). The Irminger Sea and the Iceland Sea timeseries measurements of sea water carbon and nutrient chemistry 1983–2006. *Earth Syst. Sci. Data Discuss.* 2, 477–492. doi: 10.5194/essdd-2-477-2009
- Olsen, A., Key, R. M., van Heuven, S., Lauvset, S. K., Velo, A., Lin, X., et al. (2016). The Global Ocean Data Analysis Project version 2 (GLODAPv2) – an internally consistent data product for the world ocean. *Earth Syst. Sci. Data* 8, 297–323. doi: 10.5194/essd-8-297-2016
- Pérez, F. F. (2016). Atlantic Ocean acidification. *Front. Mar. Sci. Conference Abstract: XIX Iberian Symposium on Marine Biology Studies*. doi: 10.3389/conf.FMARS.2016.05.00093
- Pérez, F. F., and Fraga, F. (2007). A precise and rapid analytical procedure for alkalinity determination. *Mar. Chem.* 21, 169–182. doi: 10.1016/0304-4203(87)90037-5
- Pérez, F. F., Vázquez-Rodríguez, M., Louarn, E., Padin, X. A., Mercier, H., and Ríos, A. F. (2008). Temporal variability of the anthropogenic CO₂ storage in the Irminger Sea. *Biogeosciences* 5, 1669–1679. doi: 10.5194/bg-5-1669-2008
- Plancherel, Y., Rodgers, K. B., Key, R. M., Jacobson, A. R., and Sarmiento, J. L. (2013). Role of regression model selection and station distribution on the estimation of oceanic anthropogenic carbon change by eMLR. *Biogeosciences* 10, 4801–4831. doi: 10.5194/bg-10-4801-2013
- Ragueneau, O., Gallinari, M., Stahl, H., Tengberg, A., Grandel, S., Lampitt, R., et al. (2001). The benthic silica cycle in the northeast Atlantic: seasonality, annual mass balance and preservation mechanisms. *Prog. Oceanogr.* 50, 171–200. doi: 10.1016/S0079-6611(01)00053-2
- Sabine, C. L., Feely, R. A., Gruber, N., Key, R. M., Lee, K., Bullister, J. L., et al. (2004). The oceanic sink for anthropogenic CO₂. *Science* 305, 367–371. doi: 10.1126/science.1097403
- Stow, C., Jolliff, J. Jr., McGillicuddy, D. J. Jr., Doney, S., Allen, J., Friedrichs, M. A. M., et al. (2009). Skill assessment for coupled biological/physical models of marine systems. *J. Mar. Syst.* 76, 4–15. doi: 10.1016/j.jmarsys.2008.03.011
- Uppström, L. R. (1974). Boron/chlorinity ratio of deep-sea water from the Pacific Ocean. *Deep Sea Res.* 21, 161–162. doi: 10.1016/0011-7471(74)90074-6
- van Heuven, S., Pierrot, D., Lewis, E., and Wallace, D. (2009). *MATLAB Program Developed for CO₂ System Calculations*. ORNL/CDIAC-105b, Carbon Dioxide Information Analysis Center, Oak Ridge National Laboratory, US Department of Energy, Oak Ridge, TN.

- Vazquez-Rodriguez, M., Perez, F. F., Velo, A., Rios, A. F., and Mercier Herle. (2012). Observed acidification trends in North Atlantic water masses. *Biogeosciences* 9, 5217–5230. doi: 10.5194/bg-9-5217-2012
- Waugh, D. W., Hall, T. M., McNeil, B. I., Key, R., and Matear, R. J. (2006). Anthropogenic CO₂ in the oceans estimated using transit time distributions. *Tellus* 58B, 376–389. doi: 10.1111/j.1600-0889.2006.00222.x
- Williams, N. L., Juranek, L. W., Johnson, K. S., Feely, R. A., Riser, S. C., Talley, L. D., et al. (2016). Empirical algorithms to estimate water column pH in the Southern Ocean. *Geophys. Res. Lett.* 43, 3415–3422. doi: 10.1002/2016GL068539
- Yashayaev, I., and Azetsu-Scott, K. (2016). *Dissolved Inorganic Carbon, pH, Alkalinity, Temperature, Salinity and Other Variables Collected From Discrete Sample and Profile Observations Using Alkalinity titrator, CTD and Other Instruments from HUDSON in the Davis Strait, Labrador Sea and North Atlantic Ocean from 2014-05-02 to 2014-05-24 (NCEI Accession 0157623)*. Version 1.1. NOAA National Centers for Environmental Information. Dataset.
- Yashayaev, I., and Loder, J. W. (2016). Recurrent replenishment of Labrador Sea water and associated decadal-scale variability. *J. Geophys. Res. Oceans* 121, 8095–8114. doi: 10.1002/2016JC012046
- Conflict of Interest Statement:** The authors declare that the research was conducted in the absence of any commercial or financial relationships that could be construed as a potential conflict of interest.
- Copyright © 2017 Turk, Dowd, Lauvset, Koelling, Alonso-Pérez and Pérez. This is an open-access article distributed under the terms of the Creative Commons Attribution License (CC BY). The use, distribution or reproduction in other forums is permitted, provided the original author(s) or licensor are credited and that the original publication in this journal is cited, in accordance with accepted academic practice. No use, distribution or reproduction is permitted which does not comply with these terms.